nature climate change

LETTERS

PUBLISHED ONLINE: 7 MARCH 2016 | DOI: 10.1038/NCLIMATE2941

More extreme precipitation in the world's dry and wet regions

Markus G. Donat[1]*, Andrew L. Lowry[1], Lisa V. Alexander[1], Paul A. O'Gorman[2] and Nicola Maher[1]

Intensification of the hydrological cycle is expected to accompany a warming climate[1,2]. It has been suggested that changes in the spatial distribution of precipitation will amplify differences between dry and wet regions[3,4], but this has been disputed for changes over land[5–8]. Furthermore, precipitation changes may differ not only between regions but also between different aspects of precipitation, such as totals and extremes. Here we investigate changes in these two aspects in the world's dry and wet regions using observations and global climate models. Despite uncertainties in total precipitation changes, extreme daily precipitation averaged over both dry and wet regimes shows robust increases in both observations and climate models over the past six decades. Climate projections for the rest of the century show continued intensification of daily precipitation extremes. Increases in total and extreme precipitation in dry regions are linearly related to the model-specific global temperature change, so that the spread in projected global warming partly explains the spread in precipitation intensification in these regions by the late twenty-first century. This intensification has implications for the risk of flooding as the climate warms, particularly for the world's dry regions.

Changes in global and regional precipitation characteristics are among the most relevant aspects of climate change in a warming world, yet there is little consensus on observed and expected changes in spatial precipitation patterns. In a warming climate, the global hydrological cycle is expected to intensify[1], although increasing aerosol concentrations might counteract this effect[2].

Globally averaged, although no robust changes in precipitation totals could be observed[9], detectable increases in precipitation extremes are found[10–12], with further increases in extremes projected for the future[13,14]. However, spatial patterns of changes are heterogeneous, with different regions showing opposing trends[15].

It has been suggested that dry regions would become drier and the wet regions wetter when considering changes in the difference between precipitation and evaporation (P − E), because atmospheric moisture convergence and divergence are expected to increase in magnitude with increasing atmospheric moisture content in a warmer atmosphere[3]. This enhancement of the pattern of P − E with warming is found to hold in global climate model (GCM) simulations on large scales over the ocean[3], consistent with observed changes in salinity[16]; but it does not hold over land[7,8], where surface moisture is limited, or locally over the ocean[7,17]. Furthermore, when classifying dry and wet regions by local precipitation amounts, such a wet-get-wetter–dry-get-drier pattern was not seen in observations over most global land areas[5,6].

Precipitation extremes may change differently from total precipitation. The simplest expectation is that precipitation extremes should scale with low-level atmospheric moisture content, which increases at a rate of about 6–7% K^{-1} warming according to the Clausius–Clapeyron relationship[18]. However, the rate of increase of precipitation extremes is affected by multiple factors, including the vertical velocity profile and its changes[19]. Scaling of subdaily precipitation extremes in the current climate at higher rates than expected from the Clausius–Clapeyron relationship has been reported for some locations[20], but the extent to which this applies to climate change remains unclear. Global-mean changes in total precipitation, by contrast, are energetically constrained and expected to increase at a lower rate[1].

In simulations of global warming, extreme precipitation intensifies in both tropical and extratropical regions[14,19]. The rate of increase with warming remains uncertain in the tropics[21], probably because of the sensitivity of simulated tropical rainfall extremes to the choice of convective parameterization[22]. Observations show that globally the number of heavy precipitation events has increased in more regions than it has decreased, although there is considerable variability in spatial trend patterns[12,15,23].

In preparation for possible future changes, it is important to understand how precipitation totals and extremes are changing in different regions. However, some degree of spatial aggregation or averaging is needed to find robust regional results, given large internal variability[24]. Instead of analysing changes for limited geographical regions[21,25], or aggregating over latitude bands[26,27], we focus on changes in spatial aggregations that represent different climatological characteristics of precipitation—focusing on the world's dry and wet regions. Similar approaches have been used previously for studying precipitation totals in wet and dry regions of the tropics[4,28]. This aggregation does not necessarily involve contiguous regions but rather includes grid cells depending on whether they are dry or wet regardless of their geographical location. Here we analyse changes in total precipitation (PRCPTOT) and annual-maximum daily precipitation (Rx1day) in the HadEX2 observational data set[15] and in GCM simulations from the Coupled Model Intercomparison Project Phase 5 (CMIP5; ref. 29). Precipitation indices are first normalized by dividing by the average of the 1951–1980 period before calculating area-weighted averages over the dry and wet grid cells, respectively (see Methods for details).

In the observational data set, 'wet' grid cells (in terms of the highest PRCPTOT and Rx1day values during the 1951–1980 climatological period) are mainly found in Southeast Asia, India, a region in eastern South America that includes southern Brazil, Uruguay and eastern Argentina, the southeastern United States, Europe, as well as small regions in northern tropical and eastern coastal Australia, eastern tropical Africa and southeastern Africa (Fig. 1c). Most of the 'dry' grid cells are located in central and northeast Asia, central Australia, northwestern North America, as

[1]Climate Change Research Centre and ARC Centre of Excellence for Climate System Science, University of New South Wales, Sydney, New South Wales 2052, Australia. [2]Massachusetts Institute of Technology, Cambridge, Massachusetts 02139, USA. *e-mail: m.donat@unsw.edu.au

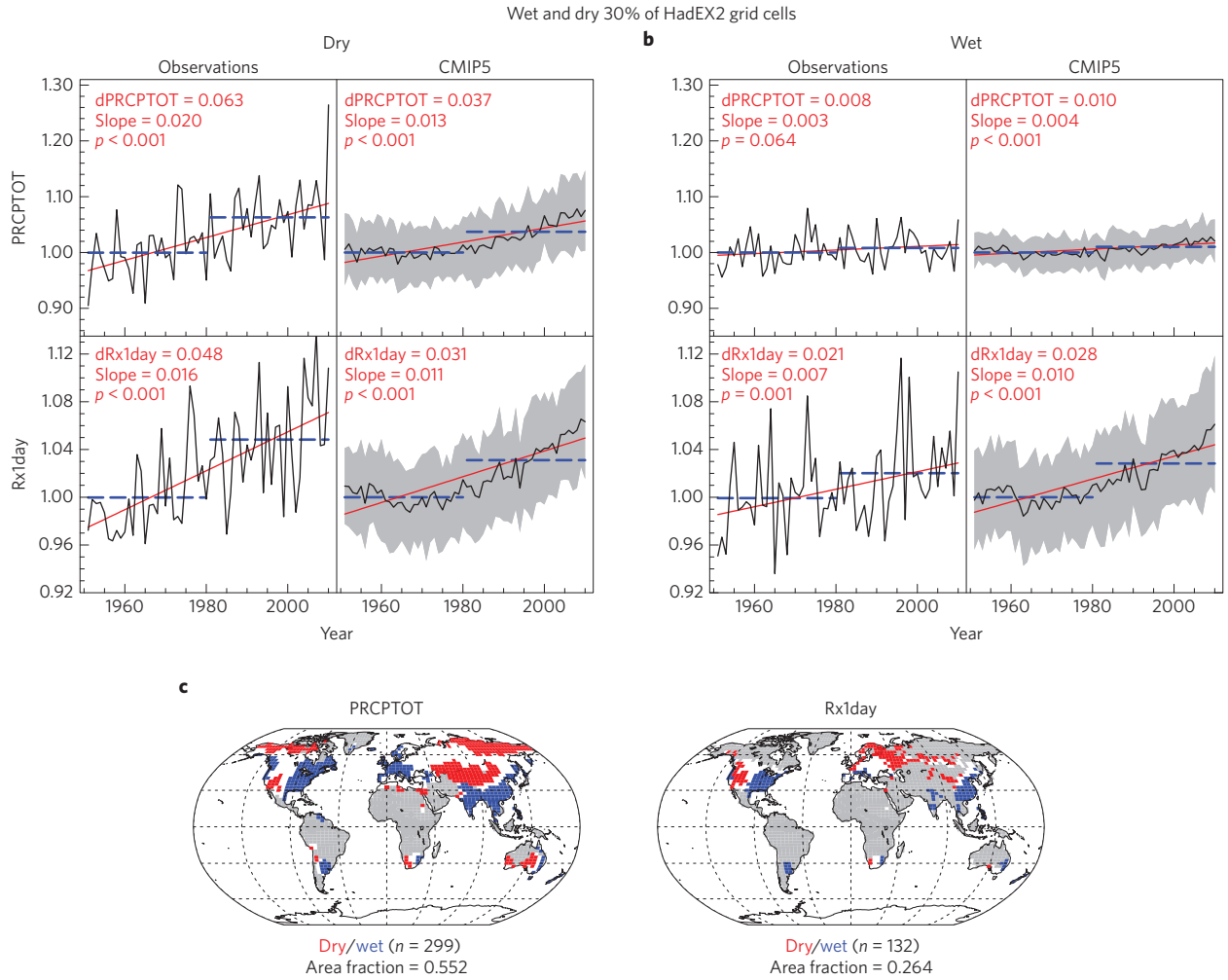

Figure 1 | Precipitation changes in the dry and wet regions identified from observations. a,**b**, Time series of PRCPTOT (annual precipitation totals) and Rx1day (the annual-maximum daily precipitation) for dry (**a**) and wet (**b**) regions in the HadEX2 observational data set. Area-weighted average time series are shown for HadEX2 and the ensemble mean and spread of CMIP5 simulations. Precipitation indices were first normalized by calculating annual values as a fraction of the 1951–1980 local mean before calculating the dry- and wet-region averages. Black lines, annual values from observations and ensemble mean; red lines, linear trend; blue dashed lines, 30-yr averages for 1951–1980 and 1981–2010; grey shading, ± one ensemble standard deviation. dPRCPTOT and dRx1day indicate the difference between the averages during 1981–2010 and 1951–1980; slope is the linear trend Sen-slope estimate (see Methods; unit, decade^{-1}); and the *p*-value is the trend significance using a Mann–Kendall test. **c**, The masks indicate the locations of the grid cells contributing to the average of the dry (red) and wet (blue) regions, and the number *n* of grid cells contributing to the area averages of dry and wet regions is given. Land grid cells that are less complete than 90% of the years 1951 to 2010 (see Methods) are coloured grey and excluded from this analysis; the masks with limited observational coverage have also been applied to the CMIP5 simulations. Area fraction indicates the fraction of land area for which data are at least 90% complete.

well as north and southwestern Africa. Note that the observational data set has large gaps (grey on the maps in Fig. 1c) over the Sahara and Amazon regions[15], for example, which would presumably contribute to the dry and wet regions, respectively.

Observations show statistically significant ($p \leq 0.05$) increases in both precipitation indices in the dry regions and in the Rx1day index in the wet regions, with slope values of 1–2% per decade (Fig. 1a,b). The slope value is weaker at 0.3% per decade for PRCPTOT in the wet regions.

The CMIP5 ensemble, when masked to the grid cells where observations are available, also shows statistically significant trends towards wetter conditions for precipitation totals and extremes. The ensemble-mean rates of increase are similar to observed rates in the wet regions, but slightly lower than in the dry regions.

Although the spatial coverage of observations is limited, change patterns for the entire globe can be analysed from the CMIP5 ensemble (Fig. 2). When considering land regions only, most of the dry grid cells are located in Saharan Africa and the Arabian Peninsula, in addition to the central and northeast Asian regions already identified in the observational data set. Also the location of the wet grid cells largely agrees with the wet regions identified from the observations, but wide regions in tropical Africa and South America are also identified when model data with complete coverage are used. The different models largely agree on the precipitation climatology spatial patterns, and generally have their dry and wet grid cells in the same regions (as indicated by the dark blue and red shades in Fig. 2c).

Ensemble-mean changes averaged over all land are very similar to the changes discussed earlier that were averaged only over areas with observational coverage, despite the fraction of land area with sufficiently complete observational coverage being only 55% for PRCPTOT and 26% for Rx1day. Again, both precipitation indices show increases of about 1–2% per decade averaged over the dry

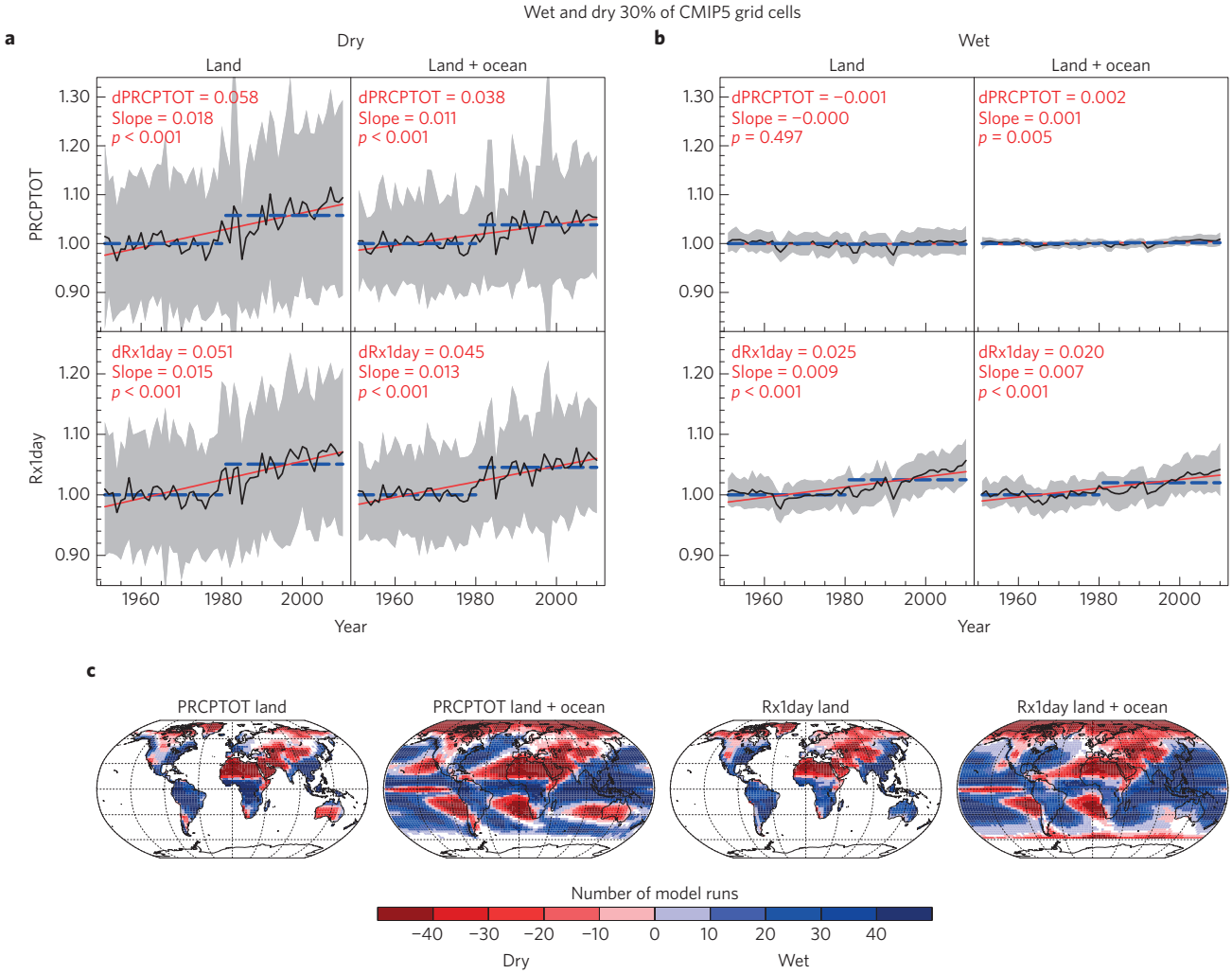

Figure 2 | Precipitation changes in the dry and wet regions identified from GCMs. a,**b**, Time series of normalized PRCPTOT and Rx1day for dry (**a**) and wet (**b**) regions in the ensemble of CMIP5 simulations. The dry and wet grid cells were identified both for land regions and for all regions (land and ocean, excluding south of 60° S). Line colours and terminology as in Fig. 1. **c**, The masks indicate counts for each grid cell of how many simulations (out of 46) have a dry/wet grid cell locally.

regions. For the wet regions, Rx1day also shows increases over the past 60 years, at a similar rate as observed, but no statistically significant change is found for PRCPTOT. Performing the analysis for all (land and ocean) grid cells (Fig. 2; see Methods), we find that changes are qualitatively similar to the changes over land only, although the rates of increase are slightly smaller. In particular for PRCPTOT in dry regions, the smaller increase when including ocean grid cells is due to decreases in some oceanic regions characterized by time-mean atmospheric moisture divergence in the current climate.

Future climate projections show strong ensemble-mean increases in total and extreme precipitation averaged over dry regions (Fig. 3). There are large inter-model uncertainties for PRCPTOT changes, with the ensemble mean $\pm$ 1 standard deviation ranging from a slight decrease (−10%) to a strong increase (+90%) by the end of the twenty-first century in the RCP8.5 scenario when ocean grid cells are included. In the wet regions the PRCPTOT increases are much smaller (below 10% by the end of the twenty-first century), and Rx1day increases are similar to projected changes analysed for dry regions.

Although there is a general tendency towards intensification of precipitation in dry and wet regions, the ensemble spread of projected changes is substantial. However, the magnitude of global warming response to increasing greenhouse gas (GHG) forcing also shows a large spread between different model simulations[30]. Therefore, we also investigate if the changes in precipitation are related to the magnitude of global warming in the different simulations.

There is a large regression coefficient (about 15% K^{-1}) for PRCPTOT in the dry land regions (Fig. 4), but the regression line does not pass close to the origin, presumably as a result of the negative fast response of precipitation to CO_2 radiative forcing, and some of the simulations give a negative PRCPTOT response. No statistically significant relationship is found for the wet-regions average. Averaging over all global grid cells, the precipitation-temperature regression slope is similar to previous studies[1,31] (Supplementary Information 6).

We also find a statistically significant relationship between daily extreme precipitation increases in dry regions and the mean temperature response in the individual model simulations. Annual extremes increase on average by between 6% (RCP4.5) and 7% (RCP8.5) per K warming—that is, close to what would be expected from the Clausius–Clapeyron relationship. Again, there is no statistically significant regression relationship for the wet regions.

Combining these results indicates a robust tendency towards greater precipitation totals and annual extremes on average over

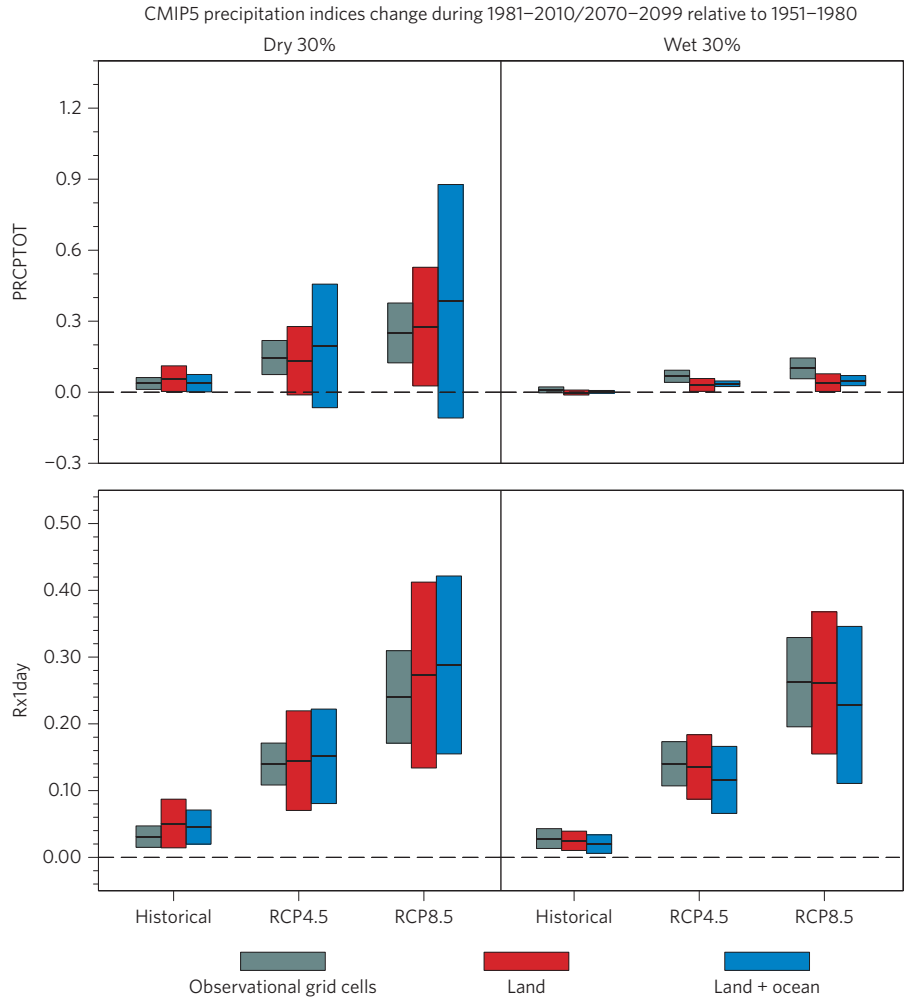

Figure 3 | Simulated precipitation changes in dry and wet regions. Precipitation index changes averaged over the dry (left column) and wet (right column) regions. Historical changes show the average during 1981–2010, and RCP4.5 and RCP8.5 show the average during 2070–2099, all relative to the 1951–1980 average. Horizontal black lines represent the ensemble-mean changes and the coloured boxes show ± one ensemble standard deviation.

the regions of the world where each is least. Total precipitation amounts and annual extremes in the dry regions are also projected to continuously increase over the twenty-first century, and there is a statistically significant relationship between the magnitude of global warming and the intensification of precipitation. Averaged over the wet regions, PRCPTOT and Rx1day increases are less robustly related to warming climate and PRCPTOT increases are comparatively lower than in the dry-regions average.

Previous studies have detected increases of precipitation extremes on global and hemispheric scales, and attributed these increases to human activities[11,32]. However, the spatial patterns of changes are complex, with regionally different trend signs. On the basis of the robustness of trends in observations and GCMs as presented here for dry regions, our results suggest that attribution of changes to anthropogenic forcings may even be robust for smaller areas when aggregated according to precipitation characteristics rather than by geographical regions. This aggregation of dry and wet regions spans different geographical regions, in which different weather patterns may govern the occurrence of extreme rain. Thus, averaging across these regions makes the time series less affected by locally relevant modes of variability[24], and leads to a higher signal-to-noise ratio in the precipitation response to global warming. Note that the dry and wet regions cover substantial parts of the globe, and although the area-average time series in most of the cases show statistically significant increases, they may contain local changes of opposing signs. Performing the same analyses separately for tropical and extratropical latitudes (Supplementary Information 3), we find the results for extratropical latitudes are very similar to the global analyses. The changes are less robust for the tropical latitudes, in particular for the dry-regions average. In most cases the ensemble spread of projected (total and extreme) precipitation changes is smallest when the analysis is restricted to areas with good observational coverage. This suggests that model uncertainties are largest in regions where we do not have good observations to compare against. In general, inter-model uncertainties in future precipitation changes are largest for tropical latitudes, particularly for PRCPTOT changes in the tropical dry regions when ocean grid cells are included (see also Supplementary Information 3).

Increasing total precipitation amounts in the dry regions may be compensated or overcompensated by increased evaporation in a warmer climate[3,7], and hence may not lead to increased water availability. We do not consider effects of evaporation in this study. This would be important for considering, for example, water balances, but of limited use for quantifying changes in precipitation extremes because the dominant balance for local heavy precipitation events is between precipitation and atmospheric moisture convergence rather than evaporation.

The increases in annual precipitation maxima are highly relevant, as they may lead to increased risk of flooding. In particular, in

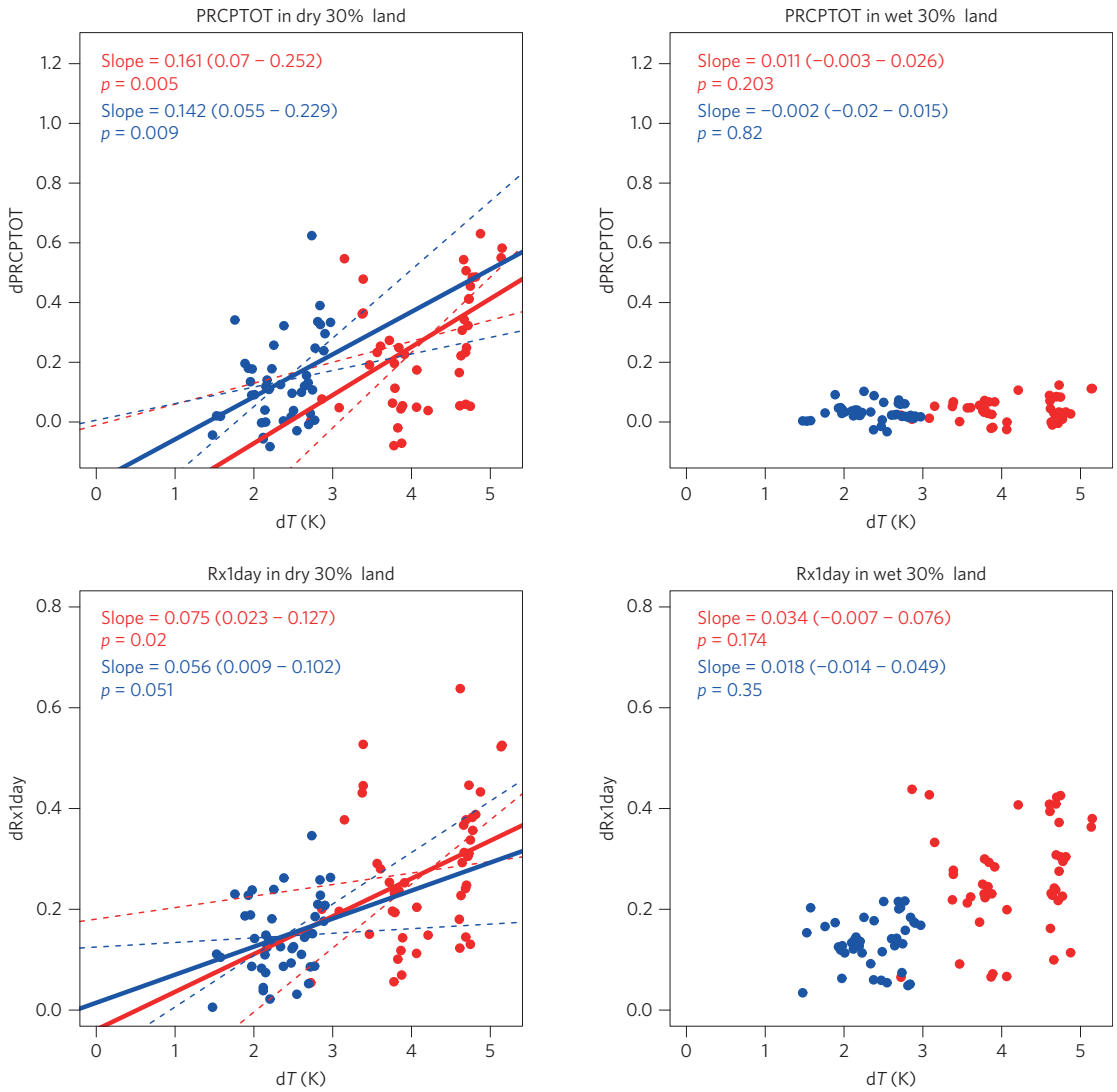

Figure 4 | Precipitation changes as a function of global warming. Scatter plots of precipitation index changes over land against global mean temperature change in the different CMIP5 simulations. Precipitation averaged over the dry (left column) and wet (right column) regions. Changes (2070–2099 minus 1951–1980) in RCP4.5 are shown in blue, and RCP8.5 in red. Dots represent the differences in the individual model runs, solid lines represent the linear regression best fit through all points of a scenario, and dashed lines represent the 5–95% uncertainty range of the linear regression slope. Regression lines are plotted only if the associated *p*-value is below or equal to 0.1.

dry regions, where high-intensity rainfall events do not usually occur, infrastructure is less well adapted to more extreme rainfall. Therefore, even small increases in the intensity of extremes can have strong impacts if no additional adaptation measures are taken.

Methods

Methods and any associated references are available in the online version of the paper.

Received 23 July 2015; accepted 20 January 2016; published online 7 March 2016

References

1. Allen, M. R. & Ingram, W. J. Constraints on future changes in climate and the hydrologic cycle. *Nature* **419,** 224–232 (2002).
2. Wu, P., Christidis, N. & Stott, P. Anthropogenic impact on Earth's hydrological cycle. *Nature Clim. Change* **3,** 807–810 (2013).
3. Held, I. M. & Soden, B. J. Robust responses of the hydrological cycle to global warming. *J. Clim.* **19,** 5686–5699 (2006).
4. Allan, R. P., Soden, B. J., John, V. O., Ingram, W. & Good, P. Current changes in tropical precipitation. *Environ. Res. Lett.* **5,** 025205 (2010).
5. Sun, F., Roderick, M. L. & Farquhar, G. D. Changes in the variability of global land precipitation. *Geophys. Res. Lett.* **39,** L19402 (2012).
6. Greve, P. *et al*. Global assessment of trends in wetting and drying over land. *Nature Geosci.* **7,** 716–721 (2014).
7. Roderick, M. L., Sun, F., Lim, W. H. & Farquhar, G. D. A general framework for understanding the response of the water cycle to global warming over land and ocean. *Hydrol. Earth Syst. Sci.* **18,** 1575–1589 (2014).
8. Byrne, M. P. & O'Gorman, P. A. The response of precipitation minus evapotranspiration to climate warming: why the 'wet-get-wetter, dry-get-drier' scaling does not hold over land. *J. Clim.* **28,** 8078–8092 (2015).
9. Trenberth, K. E. Changes in precipitation with climate change. *Clim. Res.* **47,** 123–138 (2011).
10. Alexander, L. V. *et al*. Global observed changes in daily climate extremes of temperature and precipitation. *J. Geophys. Res.* **111,** D05109 (2006).
11. Min, S-K., Zhang, X., Zwiers, F. W. & Hegerl, G. C. Human contribution to more-intense precipitation extremes. *Nature* **470,** 378–381 (2011).
12. Westra, S., Alexander, L. V. & Zwiers, F. W. Global increasing trends in annual maximum daily precipitation. *J. Clim.* **26,** 3904–3918 (2013).
13. Sillmann, J., Kharin, V. V., Zwiers, F. W., Zhang, X. & Bronaugh, D. Climate extremes indices in the CMIP5 multimodel ensemble: part 2. Future climate projections. *J. Geophys. Res.* **118,** 2473–2493 (2013).

14. Kharin, V. V., Zwiers, F. W., Zhang, X. & Wehner, M. Changes in temperature and precipitation extremes in the CMIP5 ensemble. *Clim. Change* **119,** 345–357 (2013).
15. Donat, M. G. *et al*. Updated analyses of temperature and precipitation extreme indices since the beginning of the twentieth century: the HadEX2 dataset. *J. Geophys. Res.* **118,** 2098–2118 (2013).
16. Durack, P. J., Wijffels, S. E. & Matear, R. J. Ocean salinities reveal strong global water cycle intensification during 1950 to 2000. *Science* **336,** 455–458 (2012).
17. Chadwick, R., Boutle, I. & Martin, G. Spatial patterns of precipitation change in CMIP5: why the rich do not get richer in the tropics. *J. Clim.* **26,** 3803–3822 (2013).
18. Trenberth, K. E., Dai, A., Rasmussen, R. M. & Parsons, D. B. The changing character of precipitation. *Bull. Am. Meteorol. Soc.* **84,** 1205–1217 (2003).
19. O'Gorman, P. A. & Schneider, T. The physical basis for increases in precipitation extremes in simulations of 21st-century climate change. *Proc. Natl Acad. Sci. USA* **106,** 14773–14777 (2009).
20. Westra, S. *et al*. Future changes to the intensity and frequency of short-duration extreme rainfall. *Rev. Geophys.* **52,** 522–555 (2014).
21. O'Gorman, P. A. Sensitivity of tropical precipitation extremes to climate change. *Nature Geosci.* **5,** 697–700 (2012).
22. Wilcox, E. M. & Donner, L. J. The frequency of extreme rain events in satellite rain-rate estimates and an atmospheric general circulation model. *J. Clim.* **20,** 53–69 (2007).
23. Groisman, P. Y. *et al*. Trends in intense precipitation in the climate record. *J. Clim.* **18,** 1326–1350 (2005).
24. Fischer, E. M., Beyerle, U. & Knutti, R. Robust spatially aggregated projections of climate extremes. *Nature Clim. Change* **3,** 1033–1038 (2013).
25. Lenderink, G. & van Meijgaard, E. Increase in hourly precipitation extremes beyond expectations from temperature changes. *Nature Geosci.* **1,** 511–514 (2008).
26. Allan, R. P. & Soden, B. J. Atmospheric warming and the amplification of precipitation extremes. *Science* **321,** 1481–1484 (2008).
27. Zhang, X. *et al*. Detection of human influence on twentieth-century precipitation trends. *Nature* **448,** 461–465 (2007).
28. Liu, C. & Allan, R. P. Observed and simulated precipitation responses in wet and dry regions 1850–2100. *Environ. Res. Lett.* **8,** 034002 (2013).
29. Taylor, K. E., Stouffer, R. J. & Meehl, G. A. An overview of CMIP5 and the experiment design. *Bull. Am. Meteorol. Soc.* **93,** 485–498 (2012).
30. Collins, M. *et al*. *Climate Change 2013: The Physical Science Basis* (IPCC, Cambridge Univ. Press, 2013).
31. Lambert, F. H. & Webb, M. J. Dependency of global mean precipitation on surface temperature. *Geophys. Res. Lett.* **35,** L16706 (2008).
32. Zhang, X., Wan, H., Zwiers, F. W., Hegerl, G. C. & Min, S.-K. Attributing intensification of precipitation extremes to human influence. *Geophys. Res. Lett.* **40,** 5252–5257 (2013).

Acknowledgements

This study was supported through the Australian Research Council grants CE110001028 and DE150100456. We thank the climate modelling groups contributing to CMIP5 for producing and making available their model output.

Author contributions

M.G.D. conceived the study; A.L.L., M.G.D. and N.M. performed the analyses. All authors discussed the results and contributed to writing the manuscript.

Additional information

Supplementary information is available in the online version of the paper. Reprints and permissions information is available online at www.nature.com/reprints. Correspondence and requests for materials should be addressed to M.G.D.

Competing financial interests

The authors declare no competing financial interests.

Methods

Precipitation indices from observations and global climate models. We use the HadEX2 data set[15], which provides a range of extreme temperature and precipitation indices calculated from daily station observations and interpolated on a global 2.5° × 3.75° grid. For this study, we consider two indices representing different aspects of precipitation amounts and intensity. PRCPTOT is the annual sum of all wet-day (≥1 mm) daily precipitation totals, and Rx1day is the annual-maximum daily precipitation. Only daily rainfall amounts ≥ 1 mm are used to avoid including drizzle that is overestimated in the GCM simulations[33] and also because small amounts of rainfall are under-reported, causing biases in observations[34]. Observations are analysed for the recent 60-year period 1951 to 2010. Note that spatial coverage is different for observational grids of different precipitation indices, related to different decorrelation length scales of the underlying station data (see refs 10,15). Therefore, the number of grid cells for PRCPTOT is greater than for Rx1day. Note that, despite its coarse resolution, HadEX2 reflects average station extremes, as it interpolates the local extremes rather than calculating extremes from (daily) area averages[35].

We also use the precipitation indices calculated from the GCM simulations that contributed to the Coupled Model Intercomparison Project Phase 5 (CMIP5; ref. 29). Following the same definitions as in HadEX2, the indices were calculated from daily climate model output from the historical runs[36] and future projections[13]. We use the simulations from 26 CMIP5 models (Supplementary Table 1), and include runs that provide data over the period 1951 to 2099. For each run, we merge the corresponding historical (1951–2005) and future scenario (2006–2099) simulations to give transient time series from 1951 to 2099 for both the historical plus RCP4.5 scenario and historical plus RCP8.5 scenario simulations. These scenarios describe greenhouse gas (GHG) concentration pathways, where RCP8.5 represents a future with continuing strong increase in GHG concentrations throughout the twenty-first century and RCP4.5 represents stabilization at about 575 ppm CO_2-equivalent during the second half of the century[29]. Other scenarios also exist, but the largest number of simulations in the CMIP5 archive is provided for these scenarios. Therefore, to include as many different GCMs as possible, we focus on these two scenarios. In total, we use 46 different simulations for the historical period (1951–2005) merged with RCP8.5 scenario projections (2006–2099), and 45 different simulations for historical runs merged with RCP4.5 scenario projections (2006–2099). Note that different numbers of runs are available from the different models; therefore, the models contribute with different weights to the multi-model ensemble results. The results are, however, almost identical if only one run (r1i1p1) is used from each model, so that all models have the same weight in the multi-model ensemble (Supplementary Information 2).

The calculated precipitation indices from CMIP5 were obtained from http://www.cccma.ec.gc.ca/data/climdex. All model fields were remapped to the HadEX2 grid. For the model analyses, we exclude high southern latitudes (south of 60° S), as these regions are almost uninhabited and not subject to pluvial flooding. Note that the HadEX2 observational data set does not provide data south of 60° S. For comparison of the climate model simulations with observations over the period 1951 to 2010, we merge the years 2006 to 2010 from the RCP8.5 simulations with the years 1951 to 2005 from the historical simulations. The different emission scenarios are almost identical for the first two decades of the twenty-first century, but diverge strongly towards the end of the century. Therefore, our results are insensitive to using years 2006 to 2010 from the RCP4.5 simulations instead of RCP8.5 when comparing to observations.

Calculating precipitation changes in the world's dry and wet regions. For each index, we identify the dry and wet grid cells from observations and each individual model run. Using the average over the climatological period 1951 to 1980 (that is, the first 30 years of our investigation period), we identify the grid cells with the 30 per cent lowest precipitation index values (dry) and 30 per cent highest values (wet), respectively. We also tested the robustness of our results to the choice of this 30 per cent threshold by repeating the analyses for the 20 and 40 per cent of driest and wettest grid cells, which led to very similar results in general (Supplementary Information 1), with slightly increased inter-model spread when only the driest and wettest 20 per cent of grid cells are considered. Results are also robust when Rx1day changes are calculated for the dry and wet regions identified from PRCPTOT (Supplementary Information 4).

To calculate area-average time series for the wet and dry regions, the local grid cell annual values are first normalized by dividing by the climatological mean during the 1951–1980 period. This ensures that the average is not dominated by regions with large mean values. Area averages are weighted to account for the different sizes of grid cells depending on their latitude. To minimize artificial variability from changes in spatial coverage, we only use grid cells that have at least 90% data available between 1951 and 2010.

We estimate temporal changes of the observational and CMIP5 ensemble mean time series by calculating Sen's slope estimator[37], a non-parametric method that calculates a linear fit slope as the median slope of all lines through pairs of sample points, and we estimate trend significance using the Mann–Kendall test[38]. Although the observational time series show roughly linear changes over the past 60 years (Fig. 1), we note that a linear trend is not necessarily the best fit to describe temporal changes in precipitation. Therefore, we also consider time-slice differences between the averages of the first and the last 30 years of the historical period, which leads to qualitatively similar results.

For the investigation of future projected precipitation changes, we used scenario simulations following the RCP4.5 and RCP8.5 scenarios. We note that the geographical distribution of rainfall may also change in a warming climate, and some of the past wet and dry regions may not be among the wet and dry grid cells, respectively, in the future climate. Although the results shown in the main text of the paper are based on the past wet and dry regions only, we also tested the robustness of the results when taking spatial shifts into account and performing the analyses only for grid cells that are among the dry and wet grid cells in both the past and future climate periods (Supplementary Information 5). Both approaches lead to generally similar results, but when the combined past and future mask is used the inter-model spread of projected changes is smaller compared to using only the past mask, in particular for PRCPTOT averaged over the dry regions.

Investigating precipitation changes as a function of global warming. We investigate the future projected precipitation changes as a function of global mean temperature increases. To this end, the precipitation index differences are plotted against the temperature differences calculated between the two 30-year periods, 2070–2099 relative to 1951–1980. Global average temperatures are calculated for each year as the area-weighted average of all (land and ocean) grid cells. We use ordinary least square regression to investigate whether precipitation changes are related to global temperature changes, and regression lines are plotted if the regression p-value is ≤0.1. Note that the regression lines for total precipitation are not expected to intersect the origin, because changes in radiative fluxes affect global-mean precipitation even when surface temperature does not change[1].

References

33. Stephens, G. L. *et al*. Dreary state of precipitation in global models. *J. Geophys. Res.* **115,** D24211 (2010).
34. Zhang, X. *et al*. Indices for monitoring changes in extremes based on daily temperature and precipitation data. *Wiley Interdiscip. Rev. Clim. Change* **2,** 851–870 (2011).
35. Avila, F. B. *et al*. Systematic investigation of gridding-related scaling effects on annual statistics of daily temperature and precipitation maxima: a case study for south-east Australia. *Weath. Clim. Extremes* **9,** 6–16 (2015).
36. Sillmann, J., Kharin, V. V., Zhang, X., Zwiers, F. W. & Bronaugh, D. Climate extremes indices in the CMIP5 multimodel ensemble: part 1. Model evaluation in the present climate. *J. Geophys. Res.* **118,** 1716–1733 (2013).
37. Sen, P. K. Estimates of the regression coefficient based on Kendall's Tau. *J. Am. Stat. Assoc.* **63,** 1379–1389 (1968).
38. Kendall, M. K. *Rank Correlation Methods* (Charles Griffin, 1975).